International Journal of Pharmaceutics 640 (2023) 122960

Contents lists available at ScienceDirect

International Journal of Pharmaceutics

journal homepage: www.elsevier.com/locate/ijpharm

Development of a compounded propofol nanoemulsion using multiple non-invasive process analytical technologies

T. Rooimans [a,b,*], M. Damen [c], C.M.A. Markesteijn [a], C.C.L. Schuurmans [c], N.H.C. de Zoete [a], P.M. van Hasselt [d], W.E. Hennink [b], C.F. van Nostrum [b], M. Hermes [c], R. Besseling [c], H. Vromans [a,b]

[a] Research and Development Department, Tiofarma BV, Oud-Beijerland, The Netherlands
[b] Department of Pharmaceutics, Utrecht Institute for Pharmaceutical Sciences, Utrecht University, Utrecht, The Netherlands
[c] InProcess-LSP, Oss, The Netherlands
[d] Department of Pediatrics, Wilhelmina Children's Hospital, University Medical Center Utrecht, Utrecht, The Netherlands

ARTICLE INFO

Keywords:
Propofol
Parenteral lipid nano-emulsion
COVID-19
Drug shortage
Compounding

ABSTRACT

Propofol is the preferred anaesthetic for induction and maintenance of sedation in critically ill mechanically ventilated COVID-19 patients. However, during the outbreak of the COVID-19 pandemic, regular supply chains could not keep up with the sudden increase in global demand, causing drug shortages. Propofol is formulated as an oil-in-water emulsion which is administered intravenously. This study explores the extemporaneous preparation of a propofol emulsion without specialized manufacturing equipment to temporally alleviate such shortages. A commercially available lipid emulsion (IVLE, SMOFlipid 20 %), intended for parenteral nutrition, was used to create a propofol loaded nanoemulsion via addition of liquid propofol drug substance and subsequent mixing. Critical quality attributes such as mean droplet size and the volume-weighted percentage of large-diameter (>5μm) droplets were studied. The evolution of droplet size and propofol distribution was monitored *in situ* and non-destructively, maintaining sterility, using Spatially Resolved Dynamic Light Scattering and Near Infrared Spectroscopy, respectively. Using response surface methodology, an optimum was found for a 4 % w/v propofol formulation with a ~15 min mixing time in a flask shaker at a 40° shaking angle. This study shows that extemporaneous compounding is a viable option for emergency supply of propofol drug product during global drug shortages.

1. Introduction

In early 2020, the severe acute respiratory syndrome coronavirus 2 (SARS-CoV-2) led to the outbreak of the coronavirus disease 2019 (COVID-19) pandemic. Patients infected with SARS-CoV-2 may develop acute respiratory distress syndrome (ARDS), a life-threatening form of respiratory failure (Bhatraju et al., 2020; Huang et al., 2020; Wang et al., 2020). Treatment of ARDS includes invasive mechanical ventilation which requires intensive care unit (ICU) admission. Deep sedation is often required during mechanical ventilation to reduce levels of patient anxiety, pain and agitation (Jacobi et al., 2002). Propofol is the drug of choice to achieve such sedation (Adams et al., 2020; Ammar et al., 2021). However, the sudden and drastic increase in global demand, resulted in shortages of this essential drug.

Propofol (2,6-diisopropylphenol, Fig. 1) is a highly lipophilic anaesthetic drug (Log P = 3.8, (Thompson and Goodale, 2000)), which

Abbreviations: ARDS, acute respiratory distress syndrome; ANOVA, analysis of variance; COVID-19, coronavirus disease 2019; (SR-)DLS, (spatially resolved) dynamic light scattering; DoE, design of experiments; GABA, gamma-aminobutyric acid; ICU, intensive care unit; IVLE, intravenous lipid emulsion; MA(H), marketing authorization (holder); MCT, medium chain triglycerides; NIR, near-infrared; NFS, NanoFlowSizer; OA, oleic acid; OO, olive oil; PAT, process analytical technology; PFAT5, percentage of fat residing in droplets larger than 5 μm; PDI, polydispersity index; propofol, propofol drug substance; PDP, propofol drug product propofol nanoemulsion; RMSEP, root mean square error of prediction; RVG, register verpakte geneesmiddelen (authorization number at Dutch regulatory agency); SMD, sauter mean diameter; SARS-CoV-2, severe acute respiratory syndrome coronavirus 2; SMOF, soy bean, medium chain triglyerides, olive oil, fish oil; SPOS, single particle optical sizing; USP, united states pharmacopoeia; Z_{av}, intensity weighted mean hydrodynamic size; ZS, Zetasizer Nano S.

* Corresponding author at: Research and Development Department, Tiofarma BV, Oud-Beijerland, The Netherlands.
E-mail addresses: t.rooimans@uu.nl, trooimans@tiofarma.nl (T. Rooimans).

https://doi.org/10.1016/j.ijpharm.2023.122960
Received 27 December 2022; Received in revised form 25 March 2023; Accepted 11 April 2023
Available online 13 April 2023

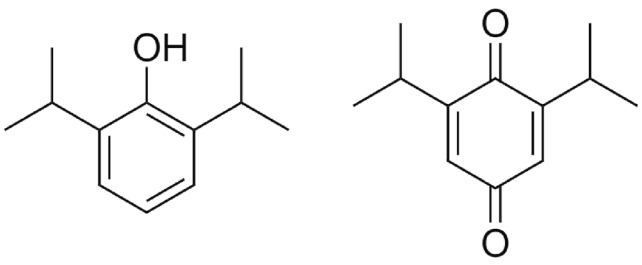

Fig. 1. Chemical structure of (**left**) propofol (2,6-diisopropylphenol) and the main oxidative degradant (**right**) impurity J (2,6-diisopropyl-1,4-benzoquinone).

easily crosses the blood–brain barrier (Baker and Naguib, 2005; Walsh, 2018). Propofol primarily acts on the gamma-aminobutyric acid (GABA) receptor, potentiating the action of the inhibitory neurotransmitter GABA, resulting in decreased signal transduction (Walsh, 2018). Sedation with propofol is fast, easily controllable and patients generally rapidly recover from its exposure due the short half-life. Rapid recovery allows for faster weaning from mechanical ventilation, which is preferred both due to ventilator associated patient health risks and to optimize ICU bed usage during high occupancy. Propofol's unique pharmacological properties make it the drug of choice to sedate mechanically ventilated patients (Jacobi et al., 2002; Shang et al., 2020).

Due to the lipophilic nature of propofol (*i.e.* oily liquid at room temperature), commercially available propofol drug products (PDPs) are formulated as parenteral lipid emulsions (Baker and Naguib, 2005). During manufacturing, propofol drug substance is first blended with an oily vehicle which is then emulsified with purified phospholipids. The resulting coarse emulsion is subsequently homogenized with a high pressure homogenizer to further reduce droplet size and narrow down the droplet size distribution. The whole procedure is typically carried out under an inert atmosphere (*e.g.* nitrogen) to protect the product against oxidation. Finally, the emulsion (*i.e.* propofol drug product) is filled under an inert atmosphere and terminally sterilized using a rotating autoclave. The production of such an emulsion is complex and requires specialized production equipment for emulsification, homogenization and sterilization. The few global manufacturers with such capabilities were not able to keep up with the sudden surge in demand.

In the Netherlands, several initiatives were taken to prevent an imminent shortage of PDP. For example, treatment guidelines were adapted to propofol sparing regimens (Landelijk Coördinatiecentrum Geneesmiddelen, 2020), PDPs were imported having a marketing authorisation outside the EU (*e.g.* South Korea, (Inspectie Gezondheidszorg en Jeugd, 2020a)) and veterinary PDPs temporarily received authorisation for human use (Inspectie Gezondheidszorg en Jeugd, 2020b). In this paper, we describe the fourth strategy: extemporaneous incorporation of propofol (*i.e.* the drug substance) to a commercially available parenteral lipid emulsion (IVLE) intended for parenteral nutrition to obtain a PDP. The feasibility of this approach was demonstrated previously (Peeters et al., 2003), but the IVLE used in that study is no longer commercially available (Table S1).

The present study uses a widely available IVLE and investigates how mixing parameters and propofol content affect emulsion quality attributes. Specific attention is given to the volume percentage of large diameter (>5 μm) droplets (PFAT5). Increased PFAT5 values are early signs of physical emulsion instability, which, for example via flocculation, coalescence, Ostwald ripening and/or creaming may lead to phase separation (Driscoll, 2015, 2006; Driscoll et al., 2001). Increased PFAT5 values are therefore linked to decreased infusion safety as the likelihood of droplet entrapment in blood capillary networks increases, potentially leading to pulmonary embolisms and/or liver damage (Driscoll, 2006; Driscoll et al., 2005). In the present study, using multiple Process Analytical Technologies (PAT), the mixing performance and propofol uptake in the emulsion was monitored non-invasively, thereby maintaining IVLE sterility (Fig. S1). Physicochemical properties of the IVLE and PDP, aspects of the mixing process relevant for the emulsion stability and PDP quality attributes were also evaluated.

2. Material and methods

2.1. Materials

The commercially available parenteral lipid emulsion used in this study was SMOFlipid 20 % (hereinafter named "IVLE", derived from "intravenous lipid emulsion") supplied in 100 ml glass bottles (Fresenius Kabi AG, Bad Homburg, Germany). The 20 % lipid fraction (w/v) in the IVLE is composed of 30 % soy bean oil, 30 % medium chain triglycerides, 25 % olive oil and 15 % fish oil. Furthermore, the formulation contains 1.2 % egg lecithin, 2.5 % glycerol, 0.02 % α-tocopherol, 0.03 % sodium oleate, (all w/v) water for injection and sodium hydroxide to pH ~8. Propofol (2,6-diisopropylphenol) with a purity of ≥ 97 % and sodium chloride were obtained from Sigma Aldrich (Burlington, MA, USA). All solvents used to make HPLC eluent were HPLC grade. Highly purified medium chain triglycerides, soybean oil and olive oil were acquired from GustavHeess GmbH (Leonberg, Germany) and purified fish oil was kindly provided by Lipoid AG (Steinhausen, Switzerland).

2.2. IVLE density

The liquid density of the IVLE was measured in triplicate using the oscillating tube principle (Densito 30PX, Mettler Toledo, Greifensee, Switzerland) at 20 °C following the equipment manufacturer's instructions.

2.3. Sample preparation

Screening experiments were conducted with 20 ml IVLE in 30 ml glass vials (Screening Devices, Amersfoort, the Netherlands). Mixing was performed using a Vortex 3 at 2500 rpm (IKA, Staufen, Germany) for a fixed duration of 10 min. Follow-up optimization studies were conducted in the original glass bottles in which the IVLE was supplied. The original fill level was maintained by removing equal volumes of blank IVLE prior to addition of the required propofol volume. Optimization studies were conducted using a SF1 flask shaker (Cole-Parmer, Stone, UK), the shaking angles varied between 0 and 180°, the operating speed was kept constant at 800 oscillations/min and the mixing time varied between 1 and 20 min. During both studies the propofol concentration ranged from 0 to 10 % w/v. The prepared emulsions were visually inspected to detect the presence of floating propofol droplets or phase separation.

2.4. Dynamic light scattering (DLS), zeta-potential and pH measurements

A Zetasizer Nano S (Malvern Instruments ltd., Malvern, UK) was used to measure hydrodynamic droplet size (Z_{av}) and polydispersity index (PDI) on samples diluted 100 × in distilled water (173° backscattering, T = 25 °C, using the refractive index and viscosity of water). Zeta-potential measurements were conducted on a Zetasizer Nano Z (Malvern Instruments ltd., Malvern, UK) and calculated from the electrophoretic mobility measured at 20 °C using the instruments dip cell with samples diluted 200 times in a 10 mM NaCl solution. The pH was measured using an Aquatrode plus electrode using a 913 pH Meter (Metrohm AG, Herisau, Switzerland) of individual samples prior to the measurement.

2.5. Spatially resolved dynamic light scattering (SR-DLS)

Spatially Resolved DLS is a recently introduced technology (NanoFlowSizer, NFS, InProcess-LSP, Oss, the Netherlands) for the non-invasive (inline and online) real-time measurement of highly turbid

nanoparticle suspensions, both under static and dynamic flow conditions (Besseling et al., 2021, 2019; Schuurmans et al., 2022). SR-DLS is based on low coherence interferometry, which uses NIR broad band light (1200–1400 nm) and measures spectral interferograms of 180° backscattered light. Fourier transformation of each interferogram yields scatter intensity resolved versus depth in the sample. High speed (~50 kHz) measurement of these profiles yields depth resolved intensity fluctuations, from which depth resolved correlation functions are acquired (Fig. S2). Multiple scattered light can thus be spatially filtered, which allows the NFS to measure Z_{av} and PDI for highly turbid, undiluted emulsions in the original IVLE glass container. In concentrated emulsions, the usual Stokes Einstein relation linking measured diffusion to droplet size (valid for dilute emulsions) requires a correction factor to account for hindered diffusion due to droplet interactions and crowding effects. This is further discussed in Section 3.5.

2.6. Diffuse reflectance near infrared Spectroscopy (DR-NIRS)

Simultaneously with the *in-situ* SR-DLS droplet size characterization, Diffuse Reflectance Near Infrared Spectroscopy (DR-NIRS) was used for the *in situ* non-invasive determination of propofol content in the original glass container (Fig. S1). DR-NIR spectra were recorded between 1000 and 2500 nm (resolution 0.25 nm) on a MPA II multi-purpose FT-NIR analyser (Bruker, Billerica, MA, USA) using a fibre optic probe. Measurements were performed with the probe positioned at half height of the container; acquisition was performed once the solution had come to rest after shaking.

2.7. Single particle optical sizing (SPOS)

Single Particle Optical Size (SPOS) was used to visualize the tail of the droplet size distribution, which allowed calculation of the volume percentage of large diameter droplets (>5 μm, PFAT5). SPOS measurements were conducted with an AccuSizer 780AD (Entegris Inc., Billerica, MA, USA) equipped with a LE400 sensor. The instrument operated in auto-dilution mode to obtain a count rate of < 9000 counts/ml and used 0.2 μm filtered distilled water as diluent. The detection threshold was set at 1.8 μm with an upper limit of 50 μm. The average results of 120, 180 and 240 s measurement durations are reported. Only the 180 s measurement results have been used as input for the Design of Experiments (DoE). The PFAT5 was calculated following the procedure outlined by Gonyon *et al* (Gonyon et al., 2007). For the calculations an oil density of 0.93 g/cm^3 (the weighted average density of the oils used in the IVLE) was used and the total fat content was expressed as the standard fat volume fraction of the IVLE ($\phi = 0.2$) plus any added propofol drug substance.

2.8. Equilibrium partition coefficient

The partition coefficient of propofol between water and the different oils was determined using the method as described by Damitz *et al.* (Damitz and Chauhan, 2015). Briefly, mixtures of propofol, oil and water were vigorously mixed for at least 72 h at room temperature (IKA multi position stirrer at 1200 rpm). The oil layer was removed each time after three consecutive centrifugation steps of 60 min at 3000*g* (20 °C). Finally, the aqueous phase was carefully removed and analysed for the propofol concentration. The partition coefficient was calculated from the aqueous drug concentration and the known masses, volumes and densities of oil and water using the following equation:

$$K = \frac{F_{prop} - \left(F_{aq}\, C_{prop} / \rho_{aq}\right)}{F_{oil}\, C_{prop} / \rho_{oil}} \quad (1)$$

Here, F_{prop}, F_{aq} and F_{oil} are the mass fractions of propofol, water and oil, respectively. C_{prop} is the aqueous propofol concentration (m/v) as determined by HPLC and ρ_{aq} and ρ_{oil} are the densities of water and the respective oil phase.

2.9. Propofol concentration

Propofol concentrations were determined using normal phase High-Performance Liquid Chromatography (HPLC) on a Shimadzu Prominence system equipped with an SPD-M20A diode array detector (Shimadzu Corp., Kyoto, Japan). Chromatographic separation was achieved on a Luna® Silica (2) (4.6 × 150 mm, 3 μm, Phenomex Inc., Torrance, CA, USA) column with an isocratic mixture of *n*-hexane: acetonitrile: anhydrous ethanol (990:7.5:1.0, v/v/v) running at 2.0 ml/min. The injected volume was 4 μl with the column and autosampler temperature set at 25 °C and 15 °C, respectively. All samples were diluted at least 25 × times in isopropyl alcohol (IPA) prior to injection. Propofol was detected at a wavelength of 271 nm. Equilibrium partition samples were analysed on a XTerra RP$_{18}$ (3.5 × 250 mm, 3 μm, Waters Corp., Milford, MA, USA) column with a mobile phase consisting of methanol: 0.05 v/v % ammonia (650: 350, v/v) running at 0.9 ml/min. The aqueous phase was directly injected (50 μl) onto the column with temperature set at 25 °C using a autosampler temperature of 20 °C. A calibration curve with known sample concentrations (~50–400 μg/ml in IPA, for RP system first dilution step in IPA thereafter mobile phase) was used to determine the sample concentration.

2.10. Response surface methodology

A response surface design (central composite) was made in Design Expert V12 (Stat-Ease, Minneapolis, USA) with propofol concentration (4–8 % w/v), shaking angle (40–80°) and shaking time (5–15 min) as the processing variables, yielding a design of 20 runs allowing to fit up to a full quadratic model (design table in Table S2). Backward model selection, starting from a full quadratic model in which terms with $p > 0.1$ were removed, was used to model the experimental results.

2.11. Terminology

For the sake of clarity, in this paper *drug substance* refers to the active pharmaceutical ingredient propofol (2,6-diisopropylphenol), whereas *drug product* refers to the finished dosage form. The term remote drug loading is used to describe the addition and incorporation (loading) of the drug substance propofol into an existing blank intravenous lipid emulsion (IVLE), thereby yielding the propofol drug product (PDP).

3. Results and discussion

3.1. IVLE selection

The preparation of a remotely loaded propofol lipid emulsion was based on the procedure previously outlined by Peeters *et al.* using Lipofundin® MCT/LCT 10 % (B. Braun Melsungen, Melsungen, Germany) (Peeters et al., 2003). This product is no longer available and of the currently available registered alternatives in the Netherlands (Table S1) SMOFlipid 200 mg/ml (hereinafter "IVLE", Fresenius Kabi AG, Bad Homburg, Germany) was deemed most suitable due to its ample supply and availability in glass bottles. Preparing a PDP in the primary IVLE packaging was highly desirable as this would yield a "simple" process where propofol can be aseptically added to the IVLE, followed by a mixing procedure to obtain the PDP. Mixing an infusion bag containing the IVLE to which propofol has been added will very likely result in poor absorption of propofol by the emulsion, especially when shaken by hand. There was a need for a solid container, such as a glass bottle (preferably with headspace), to facilitate the transfer of mechanically generated shear forces onto the emulsion during mixing.

Currently registered PDPs contain 1–2 w/v% propofol. Increasing the propofol concentration has two major benefits. First, considering that the availability of the IVLE would form the first limitation in the

studied approach, the total number of final drug products increases with increasing the propofol concentration. Secondly, as the mean duration of mechanical ventilation in COVID-19 patients ranges from 7 to 12 days there is a high risk of hypertriglyceridemia (Anesi et al., 2021; Raman et al., 2017; Saad et al., 2022). By using a more concentrated PDP the total caloric load reduces, thereby delaying the onset of hypertriglyceridemia (Raman et al., 2017).

3.2. Characterisation of blank IVLE

The density of the blank IVLE was 0.991 g/cm^3, allowing gravimetric dosing of propofol to the desired concentration (w/v%). The mean hydrodynamic diameter (Z_{av}) of the emulsion droplets in the IVLE measured by conventional DLS (Zetasizer Nano S, ZS) after 100 × dilution in RO-water was 332 ± 1 nm with a polydispersity index of 0.11 ± 0.02 (n = 3). Similarly, analysis by spatially resolved DLS (NanoFlowSizer, NFS) resulted in a Z_{av} of 369 ± 1 nm and PDI of 0.08 ± 0.01 (n = 3). This slight difference of ~35 nm in the intensity based mean size Z_{av} obtained with SR-DLS (NFS) versus conventional DLS (ZS) can be fully attributed to the differences in light source wavelength (633 nm vs 1300 nm, respectively) and angles at which light scattering is detected (173° vs 180°, respectively). Conversion to a volume based size distribution consistently yields a mean size of 415 ± 5 nm and a relative variance of 0.12 ± 0.01 for both techniques. Overall it is concluded that the measurement results of both techniques are in good agreement with each other.

The volume-weighted large-diameter fat droplets, expressed as the percentage of fat residing in droplets>5 μm (PFAT5), must be<0.05 % for parenteral lipid emulsions according to < USP 729> (United States Phamacopeial Convention, 2019). The PFAT5 of blank IVLEs was measured with SPOS and ranged between 0.0095 ± 0.0011 % and 0.0021 ± 0.0004 % depending on lot number and shelf-life.

3.3. Feasibility remote loading propofol

Propofol is easily oxidized by oxygen, by which its slightly yellow colour is transformed into deep orange due to the formation of degradation products (*i.e.* 2,6-diisopropyl-1,4-benzoquinone, Ph Eur impurity J, USP related compound B, Fig. 1). The presence of degradation products in the employed propofol drug substance (purity 98.7 ± 0.4 %, refer to Fig. S3 for typical HPLC chromatograms) aided the visual detection of residual phase separation (Fig. 2). The concentration of this impurity would be restricted to not more than 0.05 % in both the drug substance and product by the European and United States Pharmacopeia monographs.

3.3.1. Increase in droplet size

Variable quantities of propofol (1–10 %, w/v) were added to the blank IVLE in 30 ml glass vials (10 ml head space) and placed on a vortex mixer for 10 min. Visual examination did not reveal indications of remaining free (unabsorbed) propofol directly after mixing. After 48 h free oil droplets could be visually observed in the 10 % w/v propofol sample. Droplet size was measured, within 48-hours post-mixing, by conventional DLS and increased linearly with propofol content from 332 ± 1 nm to 387 ± 4 nm (Fig. 3A). Assuming that the added propofol fraction is fully taken up by the original IVLE lipid droplets, no subsequent volume contraction takes place and assuming a monodisperse emulsion, the relative change in droplet size can be calculated from volume conservation using:

$$\frac{Z_{av}}{Z_{av,0}} = \sqrt[3]{1+\frac{\phi_p(1+\phi_p)}{\phi_0}} \simeq 1+\frac{\phi_p}{3\cdot\phi_0} \quad (2)$$

Here, $Z_{av,0}$ is the initial lipid droplet size in nm, $\phi_0 = 0.2$ is the initial IVLE lipid volume fraction and ϕ_p the propofol volume fraction (refer to Supplementary material for derivation). The measured droplet size matches well with the model prediction (Fig. 3A), providing strong

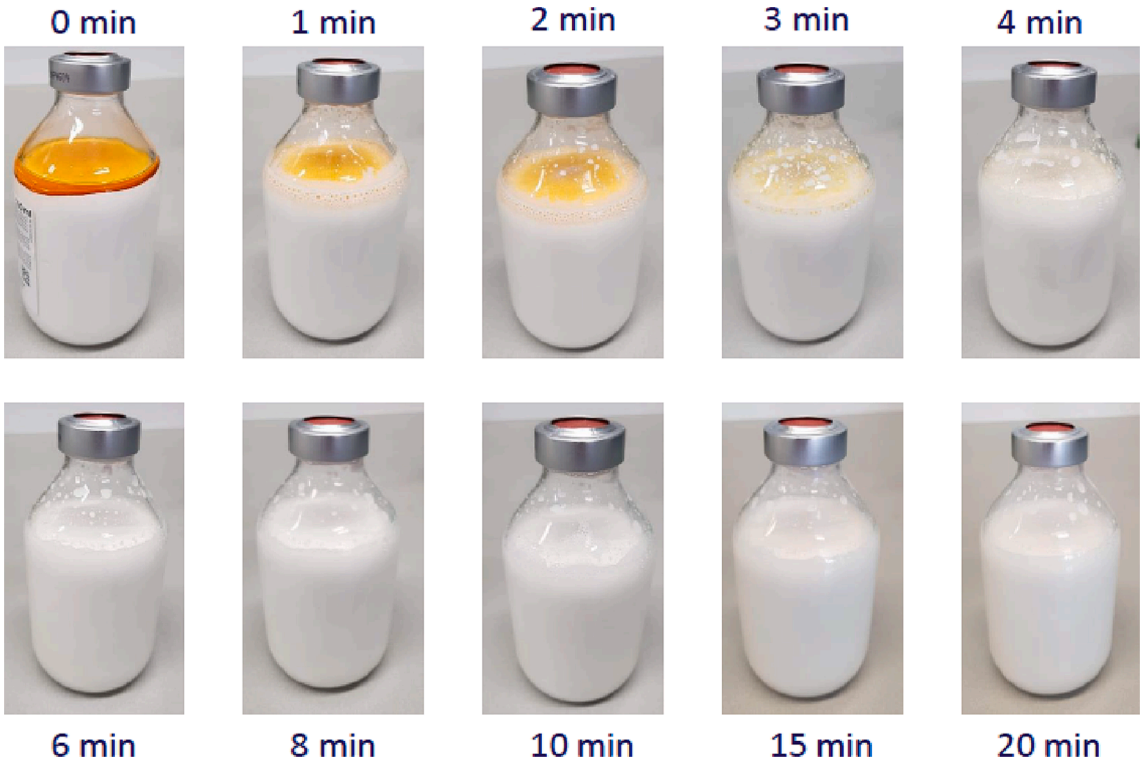

Fig. 2. Appearance of a 250 ml IVLE bottle with 6 % w/v propofol at different timepoints during exploratory mixing trials (SF1 flask shaker; 800 oscillations/min; 35° shaking angle; fill level 250 ml).

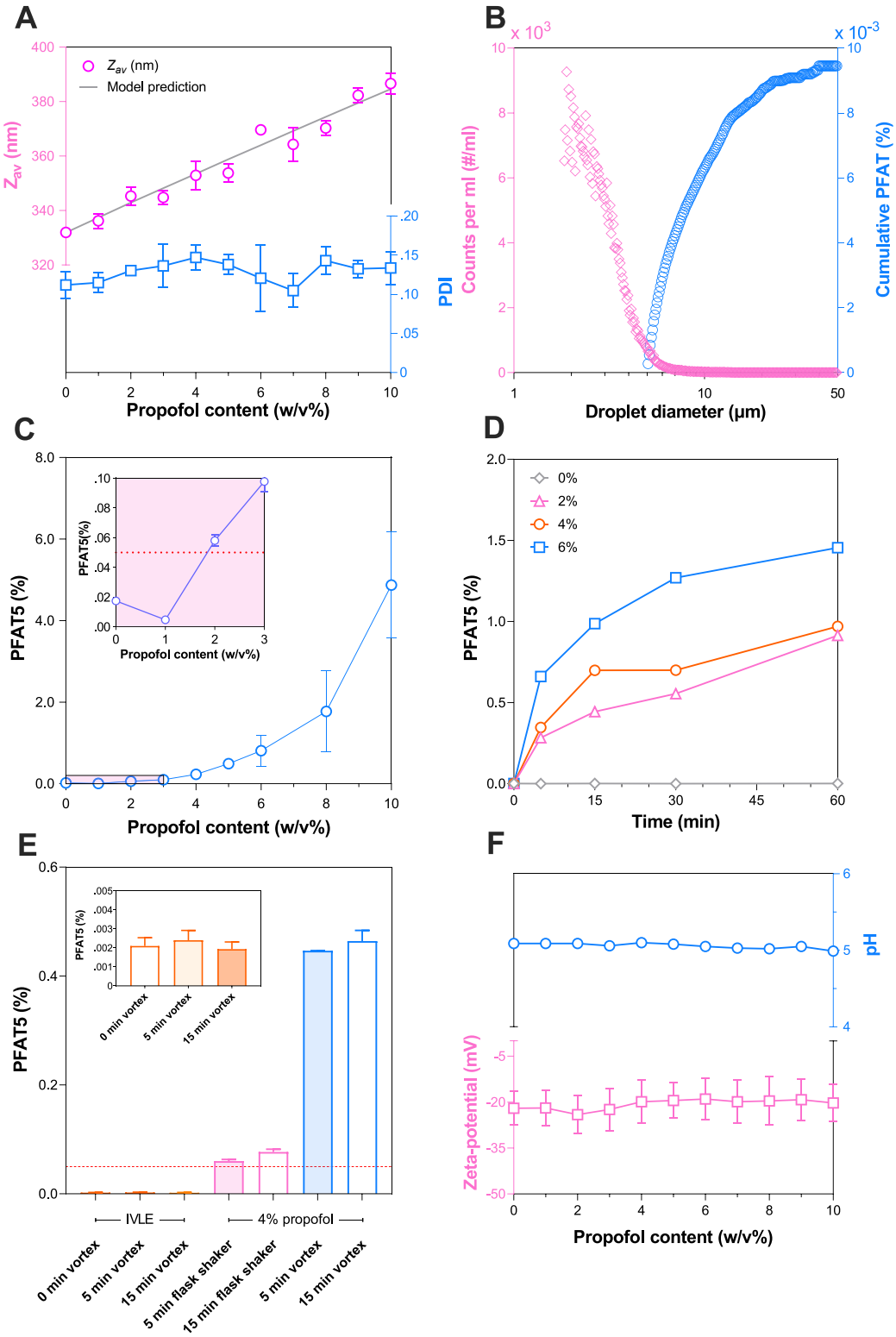

Fig. 3. A). Effect of increasing propofol concentrations (0–10 w/v%) remotely loaded into blank IVLE using a vortex mixer for 10 min on the measured and predicted hydrodynamic size (Z_{av}) and polydispersity index (PDI). **B)** Tail of the droplet size distribution of the blank IVLE expressed as the number count per millilitre (left y-axis) and cumulative PFAT (right y-axis) as determined by single particle optical sizing. **C)** Volume percentage of lipid droplets between 5 and 50 µm (PFAT5) versus propofol concentration after 10 min vortex mixing of a 20 ml emulsion in 30 ml glass vials. **D)** Evolution of PFAT5 in time from the blank IVLE remotely loaded with different propofol concentrations (0–6 % w/v) during 60 min on a multi-vortexer in 30 ml glass vials. **E)** Change in PFAT5 of the blank IVLE (inset), a 4 % w/v propofol emulsion on a SF1 flask shaker (800 oscillations/min, 0° shaking angle) and a vortex mixer (2500 rpm) both in a 100 ml glass bottle. The dashed line indicates the 0.05 % threshold value. **F)** Effect of propofol concentration on the pH and zeta-potential in 10 mM NaCl (200 × diluted). Symbols and error bars depict the mean and standard deviation (n = 3). If not shown, error bars are smaller than the symbol size except for panel B) where they are omitted for clarity and E) which has been determined individually.

evidence that propofol is absorbed by existing lipid droplets.

3.3.2. *PFAT5 increase during mixing*

Using single particle optical sensing (SPOS) the tail of the droplet size distribution could be clearly visualized for calculation of the PFAT5 (Fig. 3B). Besides an increase in droplet size (Fig. 3A), increasing the propofol content also caused a profound growth of the PFAT5 after 10 min of continuous mixing on a vortex mixer (Fig. 3C). To remain within specifications (PFAT5 < 0.05 %), it may be concluded from Fig. 3C that the maximum amount of propofol remotely loaded to the IVLE is ~2 % w/v. This is in line with currently registered propofol products, which range between 1 and 2 % w/v, but not in line with previous reports up to 6 % w/v (Peeters et al., 2003).

The data in Fig. 3C shows data as a function of propofol content and does not provide information on the potential evolution of PFAT5 as a function of mixing time. Fig. 3D shows that PFAT5 indeed grew as a

function of mixing time, with a faster increase with increasing propofol concentration. These findings are in line with previous observations by Green *et al* who showed that vigorous shaking of an IVLE increased PFAT5 (Green et al., 2014). Similarly, Han et al showed that shaking a propofol emulsion increased PFAT5 which eventually (>8 h of continuous shaking) led to the presence of free floating oil droplets (Han et al., 2001). Exploring this further, Fig. 3CDE show that the used mixing apparatus (SF1 vs vortex) and container type (30 ml glass vial vs 100 ml glass bottle) impact PFAT5 development over time as well. To understand why PFAT5 increased after complete absorption of propofol, the pH, the zeta-potential, the partition coefficient of propofol and the emulsifying capacity of the phospholipids present in in the IVLE was further studied.

Parenteral IVLEs are stabilized by a mixture of phospholipids which acts as surfactants. Depending on the IVLE generation (Table S1), they are further stabilized by the addition of sodium oleate. The majority of phospholipids in the employed IVLE (*i.e.* SMOFlipid) are phosphatidylcholine and phosphatidylethanolamine which are zwitterionic at physiological pH. However, the addition of sodium oleate and the presence of anionic phospholipids gives rise to a negative surface charge at physiological pH (Otto et al., 2018). This surface charge contributes to the colloidal stability and substances altering the pH or electrolyte balance may therefore influence the physical stability (Bhattacharjee, 2016). Propofol is a phenolic compound and thus has the potential to decrease the pH with increasing concentrations. However, Fig. 3F shows that the pH of the solution is unaffected by the addition of propofol up to 10 % w/v. The same trend is observed for the zeta-potential which remains constant at -20.7 ± 6.5 mV when diluted 200 × in 10 mM NaCl solution. Therefore, PFAT5 growth due to changes in droplet surface charge is unlikely.

The specific surface area, the area of emulsion droplets per unit volume, is given by $A_d = 6\phi / d_{3,2}$, where ϕ is the dispersed volume fraction and $d_{3,2}$ the Sauter Mean Diameter (SMD). The latter is usually obtained via laser diffraction analysis, which becomes challenging in the sub-micron range. The hydrodynamic diameter (Z_{av}) obtained by DLS may be transformed to $d_{3,2}$ via $d_{3,2} = Z_{av}/(1 + PDI)^3$ as described by Thomas (Thomas, 1987). However, this relationship only holds for small particles of unimodal size demonstrating Rayleigh scattering (typically $< 1/10$ of DLS incident wavelength). In the present case, with a Z_{av} of 332 nm, the particle size leads to Mie scattering. The DLS intensity distribution can thus be directly transformed using Mie theory to a volume distribution which in this instance leads to $Z_{av} \approx d_{3,2}$. For the blank IVLE, based on a Z_{av} of 332 nm, the specific surface area is calculated to be 3500 m^2/L. Assuming a single surfactant (LIPOID E80) concentration of 1.2 % w/v phosphatidylcholine, with an average area per molecule of 65 $Å^2$, a molecular weight of 762 g/mol and Avogadro's number an effective emulsifying area of 6100 m^2/L is obtained (Wabel, 1998). This provides a theoretical coverage of 170%, a surplus of emulsifier, possibly also explaining the presence of empty vesicles observed by transmission electron microscopy by other researchers (Placzek and Kosela, 2016; Rotenberg et al., 1991). From Fig. S4 it can be seen that the theoretical emulsifier coverage drops as a function of the propofol loading via the predicted Z_{av} (Eq. (2)). However, the emulsifier surplus is well maintained, even for propofol content up to 10 % w/v. From Fig. 3D it becomes evident that an IVLE loaded with 2 % w/v propofol already showed increased PFAT5 values. It is therefore concluded that a decreased emulsifier coverage is not the primary reason for PFAT5 growth during intensive mixing.

Although propofol is *immiscible* with water, it is not *insoluble* in water. In a 'simple' ternary mixture of propofol, oil and water, the relative aqueous propofol solubility can be assessed by determination of the partition coefficient. Commercially available IVLEs vary in their oil (and lipid) composition (Table S1) and of the four commonly used oils in IVLEs, soy bean oil had the lowest partition coefficient and Medium Chain Triglycerides (MCT) the highest, log (*K*) 3.61 versus 3.88 respectively (Table 1). Although these difference appear small, they translate to a ~2x absolute difference in the aqueous propofol solubility.

Thus an IVLE with a high proportion of MCT most effectively reduces the aqueous propofol concentration (C_{prop}). Such reduction is favourable from a clinical point of view as the free propofol concentration is associated with the intensity of pain upon injection (Baker and Naguib, 2005; Damitz and Chauhan, 2015; Klement and Arndt, 1991). But equally important, the aqueous propofol concentration (C_{prop}), can also influence physical emulsion stability as the Ostwald ripening rate increases. To explain, during Ostwald ripening larger droplets grow in time at the expense of smaller droplets which is driven by the local solubility difference between droplets varying in size. The effect of droplet radius on its surrounding solubility is given by the Kelvin equation (Tadros, 2013):

$$C(r) = C(\infty) exp\left(\frac{2\gamma V_m}{rRT}\right) \quad (3)$$

Here, $C(r)$ is the solubility surrounding a droplet of radius r, $C(\infty)$ the bulk solubility, γ the interfacial tension, V_m the molar volume of the dispersed phase, R the gas constant and T the absolute temperature. Ostwald ripening is described by the Liftshitz and Slyozoz and Wagner (LSW) theory (Wooster et al., 2008). The Ostwald ripening rate, ω, is given by:

$$\omega = \frac{d\langle r\rangle^3}{dt} = \frac{8}{9}\left[\frac{C(\infty)\gamma V_m D}{\rho_{oil} RT}\right] \quad (4)$$

Here, D is the diffusion coefficient of the dispersed phase and ρ_{oil} the density of the dispersed phase. Thus, in the 'classical representation' of the LSW theory, Ostwald ripening is a diffusion mediated process at rest, for example as experienced by the formulation during shelf life. It has been demonstrated that concurrent convective flow (at low Reynolds number) gives a significant increase in the rate of Ostwald ripening, which may be explained by droplet movement due to flow rather than solely diffusion-driven movement (Ratke and Thieringer, 1985). It is hypothesized, that during intensive mixing (at high Reynolds number), Ostwald ripening may be further accelerated.

3.3.3. Interim conclusion

Based on the above findings it is concluded that remote loading of propofol in a blank IVLE via vortex mixing is indeed possible. When the oily propofol has been added, the PFAT5 will first decrease over mixing time, caused by absorption of propofol in existing lipid droplets. Prolonged mixing, after propofol has been fully absorbed, results in a subsequent increase in PFAT5. In order to prevent excessive increase of the PFAT5, processing and formulation variables need to be balanced to find an optimum between mixing efficiency and the risk of overmixing.

3.4. Mixing process development

To study process and formulation settings in a multi-factorial way on the PFAT5, response surface methodology was applied. The goal of the optimization process was not to characterize the entire region of operability, but to find the optimum processing conditions. Exploratory experiments confirmed a large impact of the shaking angle on the rate of PFAT5 change (Fig. S5).The region of interest for the shaking angle was therefore narrowed to $40 - 80°$. The input concentration range was set

Table 1
Partition coefficients of propofol between water and the various oils which are used in the IVLE.

Matrix	Partition coefficient (log_{10} K)
Olive oil, refined	3.65 ± 0.05
Soy bean oil, purified	3.61 ± 0.02
Fish oil, purified	3.73 ± 0.03
Medium Chain Triglycerides	3.88 ± 0.11

at 4–8 % w/v propofol and based on visual assessment of the mixing process (Fig. 2), the minimum and maximum shaking durations were set at 5 and 15 min, respectively.

The results in Figs. S5 and S6 show that the residuals (error) were a function of the magnitude of the response, therefore the data was transformed by taking the inverse of the response. By design, the experimental model was capable of fitting up to a full quadratic model, however some higher order cubic terms could be included as they were net aliased with other terms. A reduced cubic model resulted in the best fit of the data which was highly significant ($p < 0.0001$) with a non-significant lack of fit (0.0688). The model R-squared value ($R^2 = 0.9353$) closely agrees with the adjusted R-squared ($R^2_{adj} = 0.8883$) which is corrected for the amount of model terms. The predicted R-squared indicates how well the model predicts new observations and indicates a reasonable predictive value ($R^2_{pred} = 0.6699$). To maintain hierarchy in the model, the main effect 'time' was included although not significant on its own ($p = 0.1750$). The fit parameters and results from the ANOVA are displayed in Table S3. The final equation in terms of coded factors is given by:

$$1/\mathrm{PFAT5} = 20.75 + -4.13 * \mathrm{A} + -2.10 * \mathrm{B} + 1.01 * \mathrm{C} + 2.75 * \mathrm{AB} + -5.32 * \mathrm{BC} + -3.42 * \mathrm{B2} + -2.52 * \mathrm{C}^2 + -2.56 * \mathrm{AB2} \quad (5)$$

By expressing the equation in coded factors (low = -1, high = +1) a direct comparison between coefficients (Table S3) is possible. This equation shows that PFAT5 is especially dependent on the propofol concentration (A) and the interaction between the shaking angle (B) and shaking duration (C). Fig. 4 shows model graphs presenting all parent terms and their relative interaction.

From Fig. 4 it is concluded that a 4 % w/v propofol formulation in a SF1 flask shaker at a 40° angle for 15 min would provide the most desirable outcome in terms of the lowest PFAT5. However, when the criteria of PFAT5 is not>0.05 % is maintained other combinations are also possible. For example, 6 % propofol at a shaking angle between 40 and 55°.

3.5. Process analytical Technologies (PAT)

When propofol is aseptically added to an individual glass container and mixed, each container constitutes an unique batch. Classical in-process controls or quality control of the end product would require opening of each bottle, voiding the sterility requirements of the formulation. Therefore, it was desirable to employ non-destructive measurement (PAT) techniques to monitor the evolution of droplet size and distribution of propofol. This was realized by simultaneous DR-NIR and SR-DLS measurements (Fig. S1).

To determine the propofol concentration non-invasively, a DR-NIR calibration curve was established based on the second derivative NIR spectra (Fig. 5). Variable quantities (0–10 % w/v) of propofol were added to the blank IVLE in 10 ml glass vials (8 ml head space) and placed on a vortex mixer for 5 min. The calibration curve was constructed using the peak at 1688 nm, related to aromatic C—H bending vibrations, abundantly present in propofol (Mizushima et al., 2011; Wilson et al., 2015). This peak was selected for further evaluation as it correlated well with the propofol content and showed negligible contribution of the IVLE. A single wavelength linear regression model at 1688 nm was obtained with R-squared 0.9988, a Root Mean Square Error of Prediction (RMSEP) of 0.04 % absolute and 0.7 % relative (Fig. 5C). These results indicate excellent model predictive capacity to quantitatively assess the propofol content directly through the IVLE glass container.

Simultaneously with the DR-NIR content measurement, SR-DLS was used to measure the size of the emulsion droplets in through the IVLE glass container in a non-invasive way. First an offline calibration was performed to account for the hindered diffusion in concentrated emulsions. The dilution series for a 4 % w/v propofol content emulsion in Fig. 6A demonstrates that the *apparent* size Z^*_{av} (~660 nm) in the undiluted emulsion decreased by ~40 % to a plateau (>50x dilution) representing the actual droplet Z_{av}. The latter increased linearly with the propofol concentration (Fig. 6B, left axis). The *apparent* Z^*_{av}, normalized by its value in the pure IVLE ($Z^*_{av,0}$), also increased linearly with the propofol concentration (Fig. 6B, right axis). The evolution of droplet size in the undiluted system can thus be directly followed by $Z^*_{av}/Z^*_{av,0}$ as a function of time.

The combined SR-DLS and DR-NIR data for relative droplet size and propofol concentration of a 4 % w/v propofol sample mixed for 15 min in the SF1 Flask shaker at a 40° shaking angle is shown in Fig. 6C-D. The largest change was observed within the first five minutes, whereafter both the propofol content and Z_{av} plateaued. Exponential fits to the data resulted in a reasonable fit for droplet size evolution ($R^2 = 0.8371$) and an excellent fit for the propofol content ($R^2 = 0.9988$) as a function of time (Fig. 6C-D).

Finally, short term physical stability was studied for the 4 % w/v formulation during 14 days at room temperature. Over time a slightly yellow coloured band appeared at the surface which was too small to analyse with DR-NIR. Samples were therefore withdrawn at different positions (top, middle and bottom) from the glass container and analysed offline by HPLC. A gradient was found from top to bottom: top 118.6 %, middle 100.1 % and bottom 93.9 % (Fig. S7). The Brownian

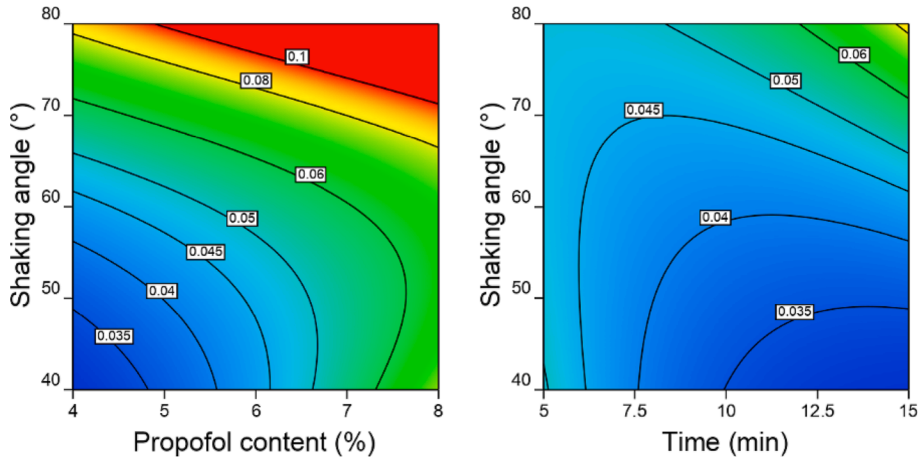

Fig. 4. 2D response surface contour plots of the AB (left) and BC (right) interactions on PFAT5, indicated by the labels of the contour lines, ranging from 0.03 to 0.1. **Left**) propofol content (%w/v) versus the shaking angle (°) with time fixed at 15 min and **right**) time (min) versus shaking angle (°) with propofol content fixed at 4% (w/v).

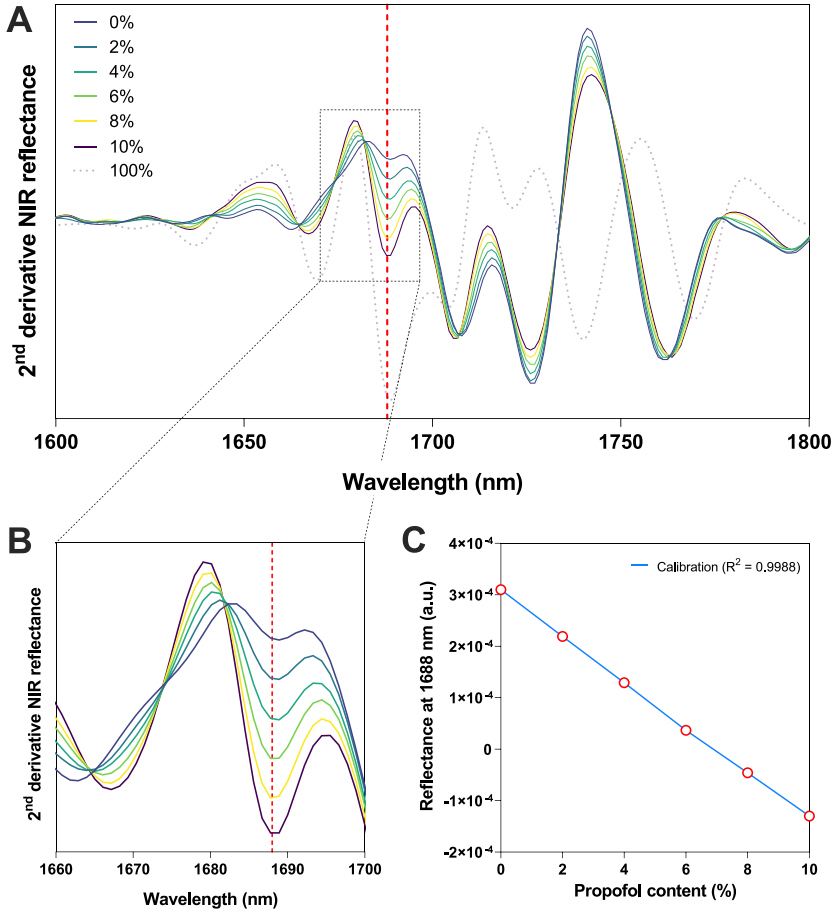

Fig. 5. Overview of the second-derivative NIR reflection spectra of pure propofol and the IVLE remotely loaded with 0–10 % (w/v) propofol over the **A)** 1600–1800 nm region. **B)** Zoom-in of the 1660–1700 nm region **C)** Results of linear regression analysis for propofol content versus reflectance intensity at 1688 nm ($R^2 = 0.9988$, RMSEP: absolute 0.04 %, relative 0.07 %).

motion of the lipid droplets was insufficient to overcome gravitational separation (creaming) over time. The reversible nature of this process was clearly demonstrated by gently shaking the sample bottles: top 100.5 %, middle 99.4 % and bottom 99.5 % (Fig. S7). Creaming of IVLEs is an intrinsic property of such emulsions and underscores the need for gentle shaking prior to administration, which is in line with the manufactures instructions (Chi and Rice, 2016; Damitz and Chauhan, 2015).

3.6. Perspective

In this study we have illustrated how a blank IVLE can be loaded with a lipophilic drug to transform it into a drug carrier. Although this paper focusses on propofol as a drug substance, other lipophilic drugs could benefit from the same approach. Key selection criterium for the drug substance is a high solubility in the dispersed oily phase, typical drug substances which are likely to be suitable are vitamin k, ubiquinone, idebenone, diazepam, amphotericin, paclitaxel and cyclosporine. The benefit of propofol is its low melting point, allowing easy addition to the IVLE via a syringe. Drug substances which are in their solid state at room temperature, may first need to be dissolved in an oily co-solvent. Although the manufacturing process of the blank IVLE is complex, converting it into a drug carrier is - as demonstrated in the present study - straightforward and does not require expensive equipment and or infrastructure.

Due to the non-invasive nature of both PAT techniques key quality attributes of the final drug product could be measured without compromising the sample integrity. NIR spectroscopy has already the status of being an industry standard PAT solution. In this work we have, for the first time, demonstrated the dual use with a novel secondary PAT technique (*i.e.* SR-DLS). Most often DLS is performed offline in a laboratory environment, meaning that the sample integrity will be compromised during sampling. DLS techniques are also available offering in-line and at-line particle size and distribution analysis, often after automated sample dilution. Although this might work in a manufacturing process where the drug product is produced in bulk, it this does not work in the presented remote loading strategy of a blank IVLE in a glass bottle. This is where the unique capabilities of SR-DLS come into play (Fig. S2). SR-DLS is capable of measuring highly turbid dispersions under flow, which is impressive as the measurement principle of normal DLS relies on Brownian motion. This provides the possibility of integrating the technology online for real-time particle size feedback. SR-DLS strongly distinguishes itself as an online PAT technique during a manufacturing process, in the current work it was used as a static and offline analysis tool but without compromising the sample integrity.

4. Conclusion

In this paper, preparation of propofol emulsions via simple remote loading and subsequent mixing of propofol in a widely available IVLE (SMOFlipid 200 mg/ml) was studied. By assessment of different mixing protocols, the influence of propofol content and physicochemical properties of the IVLE relevant for emulsion quality (PFAT5), it was shown that extemporaneous preparation (at 4 w/v% propofol) is a viable option to rapidly obtain propofol emulsions, for example during emergency drug product shortages. The combination of two PAT

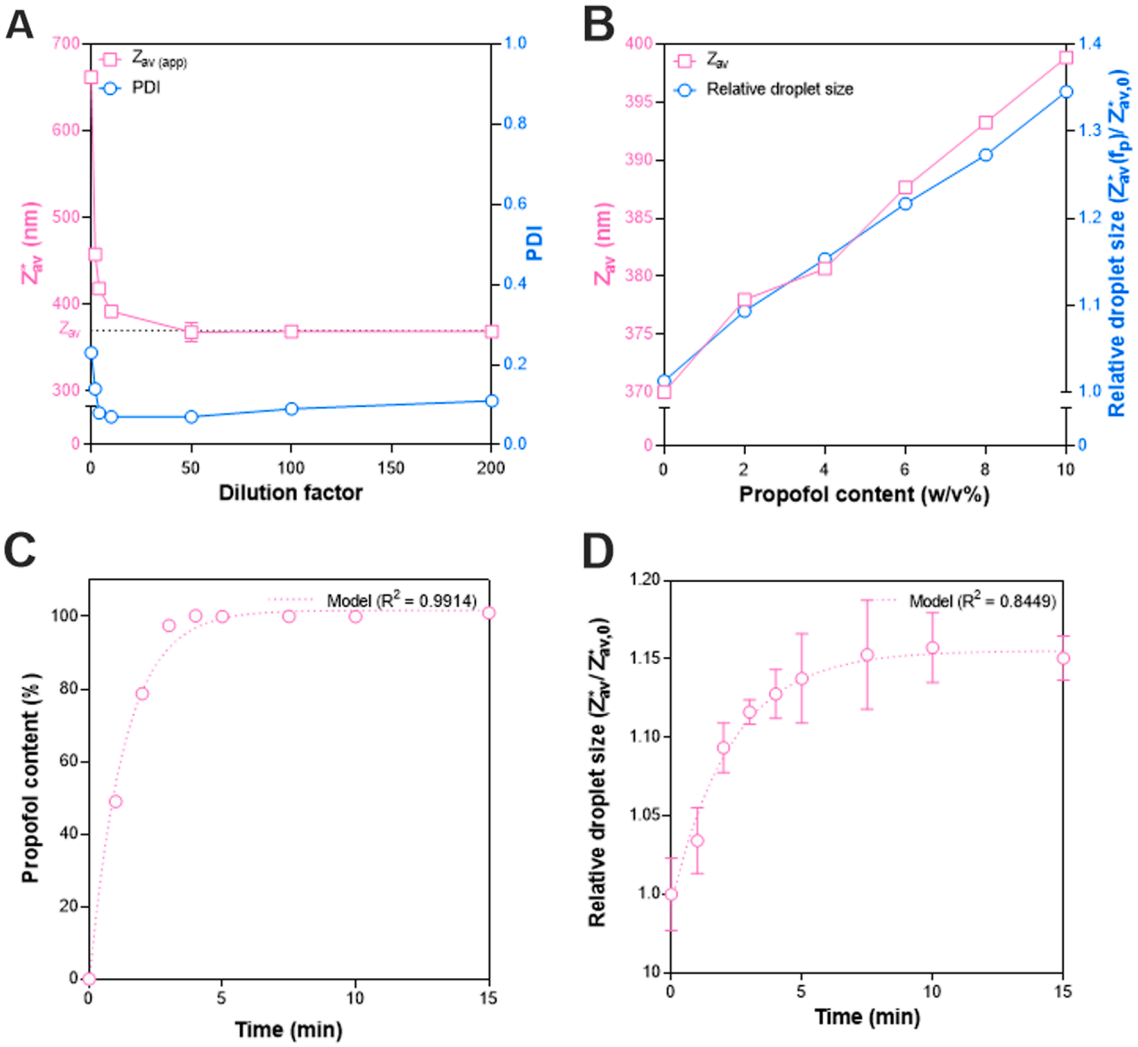

Fig. 6. A) Effect of dilution on the Z_{av} and PDI of a 4 % w/v propofol emulsion measured by SR-DLS. **B)** Effect of increasing propofol concentrations (0–10 w/v%) remotely loaded into blank IVLE lipid droplets using a vortex mixer for 10 min on the diluted Z_{av} (200 × RO-water) and normalized *apparent* size $Z^*_{av}(f_p)/Z^*_{av,0}$ measured directly in the undiluted emulsion. **C)** Evolution of propofol concentration as a function of time measured with DR-NIR at the middle of the flask. **D)** Normalized droplet size $Z^*_{av}/Z^*_{av,0}$ as a function of time for a 4 % w/v remotely loaded propofol emulsion in the SF1 flask shaker at a 40° shaking angle. Symbols and error bars depict the mean and standard deviation (n = 3), if no error bars are shown the value is smaller than the symbol value.

techniques, DR-NIR and the novel SR-DLS technique, eliminated the need for destructive sampling whilst still allowing quality control of individual containers on two critical quality attributes, namely propofol distribution and droplet size distribution.

Funding

This research did not receive any specific grant from funding agencies in the public, commercial, or not-for-profit sectors.

6. Disclaimer

The information contained in this manuscript is not a formal dissemination or information by Tiofarma and does not represent the company's position or policy.

CRediT authorship contribution statement

T. Rooimans: Conceptualization, Formal analysis, Investigation, Methodology, Visualization, Writing – original draft, Writing – review & editing. **M. Damen:** Investigation, Visualization, Writing – review & editing. **C.M.A. Markesteijn:** Investigation, Visualization, Writing – review & editing. **C.C.L. Schuurmans:** Formal analysis, Investigation, Visualization, Writing – original draft, Writing – review & editing. **N.H. C. de Zoete:** Investigation, Writing – review & editing. **P.M. van Hasselt:** Writing – review & editing. **W.E. Hennink:** Writing – review & editing. **C.F. van Nostrum:** Writing – review & editing. **M. Hermes:** . **R. Besseling:** Formal analysis, Investigation, Methodology, Visualization, Writing – original draft, Writing – review & editing. **H. Vromans:** Conceptualization, Methodology, Supervision, Writing – review & editing.

Declaration of Competing Interest

The authors declare that they have no known competing financial interests or personal relationships that could have appeared to influence the work reported in this paper.

Data availability

Data will be made available on request.

Appendix A. Supplementary material

Supplementary data to this article can be found online at https://doi.org/10.1016/j.ijpharm.2023.122960.

References

Adams, C.D., Altshuler, J., Barlow, B.L., Dixit, D., Droege, C.A., Effendi, M.K., Heavner, M.S., Johnston, J.P., Kiskaddon, A.L., Lemieux, D.G., Lemieux, S.M., Littlefield, A.J., Owusu, K.A., Rouse, G.E., Thompson Bastin, M.L., Berger, K., 2020. Analgesia and sedation strategies in mechanically ventilated adults with COVID-19. Pharmacotherapy 40, 1180–1191. https://doi.org/10.1002/PHAR.2471.

Ammar, M.A., Sacha, G.L., Welch, S.C., Bass, S.N., Kane-Gill, S.L., Duggal, A., Ammar, A. A., 2021. Sedation, analgesia, and paralysis in COVID-19 patients in the setting of drug shortages. J. Intensive Care Med. 36, 157–174. https://doi.org/10.1177/0885066620951426.

Anesi, G.L., Jablonski, J., Harhay, M.O., Atkins, J.H., Bajaj, J., Baston, C., Brennan, P.J., Candeloro, C.L., Catalano, L.M., Cereda, M.F., Chandler, J.M., Christie, J.D., Collins, T., Courtright, K.R., Fuchs, B.D., Gordon, E., Greenwood, J.C., Gudowski, S., Hanish, A., William Hanson, I., Heuer, M., Kinniry, P., Kornfield, Z.N., Kruse, G.B., Lane-Fall, M., Martin, N.D., Mikkelsen, M.E., Negoianu, D., Pascual, J.L., Patel, M.B., Pugliese, S.C., Qasim, Z.A., Reilly, J.P., Salmon, J., Schweickert, W.D., Scott, M.J., Shashaty, M.G.S., Sicoutris, C.P., Wang, J.K., Wang, W., Wani, A.A., Anderson, B.J., Gutsche, J.T., 2021. Characteristics, outcomes, and trends of patients With COVID-19-related critical illness at a learning health system in the United States. Ann. Intern. Med. 174, 613–621. https://doi.org/10.7326/M20-5327.

Baker, M.T., Naguib, M., 2005. Propofol: the challenges of formulation. Anesthesiology 103, 860–876. https://doi.org/10.1097/00000542-200510000-00026.

Baker, M.T., Naguib, M., 2005. Propofol: The challenges of formulation. Anesthesiology 103, 860–876. https://doi.org/10.1097/00000542-200510000-00026.

Besseling, R., Damen, M., Wijgergangs, J., Hermes, M., Wynia, G., Gerich, A., 2019. New unique PAT method and instrument for real-time inline size characterization of concentrated, flowing nanosuspensions. Eur. J. Pharm. Sci. 133, 205–213. https://doi.org/10.1016/J.EJPS.2019.03.024.

Besseling, R., Arribas-Bueno, R., Tuijn, R., Gerich, A., 2021. Real-Time Droplet Size Monitoring of Nano Emulsions [WWW Document]. Available from: <https://www.azonano.com/article.aspx?ArticleID=5679> (accessed 11.17.22).

Bhatraju, P.K., Ghassemieh, B.J., Nichols, M., Kim, R., Jerome, K.R., Nalla, A.K., Greninger, A.L., Pipavath, S., Wurfel, M.M., Evans, L., Kritek, P.A., West, T.E., Luks, A., Gerbino, A., Dale, C.R., Goldman, J.D., O'Mahony, S., Mikacenic, C., 2020. Covid-19 in critically Ill patients in the Seattle region - case series. N. Engl. J. Med. 382, 2012–2022. https://doi.org/10.1056/NEJMOA2004500.

Bhattacharjee, S., 2016. DLS and zeta potential - What they are and what they are not? J. Control. Release 235, 337–351. https://doi.org/10.1016/J.JCONREL.2016.06.017.

Chi, M.H., Rice, M.J., 2016. Propofol: to shake or not to shake. Rom. J. Anaesth. intensive care 23, 5–6. https://doi.org/10.21454/RJAIC.7518.231.PPF.

Damitz, R., Chauhan, A., 2015. Kinetically stable propofol emulsions with reduced free drug concentration for intravenous delivery. Int. J. Pharm. 486, 232–241. https://doi.org/10.1016/J.IJPHARM.2015.03.057.

Driscoll, D.F., 2006. Lipid injectable emulsions: pharmacopeial and safety issues. Pharm. Res. 23, 1959–1969. https://doi.org/10.1007/S11095-006-9092-4.

Driscoll, D.F., 2015. Commercial lipid emulsions and all-in-one mixtures for intravenous infusion - composition and physicochemical properties. World Rev. Nutr. Diet. 112, 48–56. https://doi.org/10.1159/000365430.

Driscoll, D.F., Etzler, F., Barber, T.A., Nehne, J., Niemann, W., Bistrian, B.R., 2001. Physicochemical assessments of parenteral lipid emulsions. Int. J. Pharm. 219, 21–37. https://doi.org/10.1016/s0378-5173(01)00626-3.

Driscoll, D.F., Ling, P.R., Quist, W.C., Bistrian, B.R., 2005. Pathological consequences from the infusion of unstable lipid emulsion admixtures in guinea pigs. Clin. Nutr. 24, 105–113. https://doi.org/10.1016/j.clnu.2004.07.022.

Gonyon, T., Patel, P., Owen, H., Dunham, A.J., Carter, P.W., 2007. Physicochemical stability of lipid injectable emulsions: correlating changes in large globule distributions with phase separation behavior. Int. J. Pharm. 343, 208–219. https://doi.org/10.1016/J.IJPHARM.2007.05.038.

Green, J.B.D., Carter, P.W., Zhang, Y., Patel, D., Kotha, P., Gonyon, T., 2014. Automated system for kinetic analysis of particle size distributions for pharmaceutically relevant systems. J. Anal. Methods Chem. 2014 https://doi.org/10.1155/2014/810589.

Han, J., Davis, S.S., Washington, C., 2001. Physical properties and stability of two emulsion formulations of propofol. Int. J. Pharm. 215, 207–220. https://doi.org/10.1016/S0378-5173(00)00692-X.

Huang, C., Wang, Y., Li, X., Ren, L., Zhao, J., Hu, Y., Zhang, L., Fan, G., Xu, J., Gu, X., Cheng, Z., Yu, T., Xia, J., Wei, Y., Wu, W., Xie, X., Yin, W., Li, H., Liu, M., Xiao, Y., Gao, H., Guo, L., Xie, J., Wang, G., Jiang, R., Gao, Z., Jin, Q., Wang, J., Cao, B., 2020. Clinical features of patients infected with 2019 novel coronavirus in Wuhan, China. Lancet (London, England) 395, 497–506. https://doi.org/10.1016/S0140-6736(20)30183-5.

Inspectie Gezondheidszorg en Jeugd, 2020a. Besluit Inspectie Gezondheidszorg en Jeugd van 26 maart 2020, kenmerk 2020-2474436 / IT2032699, houdende het verlenen van toestemming voor het afleveren van een geneesmiddel zonder handelsvergunning in Nederland vanwege een tekort van Propofol, 10 mg/mL, [WWW Document]. Available from: <http://www.rijksoverheid.nl/ministeries/vws/bezwaarschriften-vws> (accessed 11.17.22).

Inspectie Gezondheidszorg en Jeugd, 2020b. Sedatiemiddel met propofol voor dieren tijdelijk ook toegestaan voor mensen op IC's; veiligheid en kwaliteit gegarandeerd | Nieuwsbericht | Inspectie Gezondheidszorg en Jeugd [WWW Document]. Available from: <https://www.igj.nl/actueel/nieuws/2020/04/03/sedatiemiddel-met-propofol-voor-dieren-tijdelijk-ook-toegestaan-voor-mensen-op-ic's-veiligheid-en-kwaliteit-gegarandeerd> (accessed 11.17.22).

Jacobi, J., Fraser, G.L., Coursin, D.B., Riker, R.R., Fontaine, D., Wittbrodt, E.T., Chalfin, D.B., Masica, M.F., Bjerke, H.S., Coplin, W.M., Crippen, D.W., Fuchs, B.D., Kelleher, R.M., Marik, P.E., Nasraway, S.A., Murray, M.J., Peruzzi, W.T., Lumb, P.D., 2002. Clinical practice guidelines for the sustained use of sedatives and analgesics in the critically ill adult. Crit. Care Med. 30, 119–141. https://doi.org/10.1097/00003246-200201000-00020.

Klement, W., Arndt, J.O., 1991. Pain on injection of propofol: effects of concentration and diluent. Br. J. Anaesth. 67, 281–284. https://doi.org/10.1093/BJA/67.3.281.

Landelijk Coördinatiecentrum Geneesmiddelen, 2020. Prognose verbruik propofol [WWW Document]. Available from: <https://nvza.nl/wp-content/uploads/2020/06/LCG-Alert-Schaarste-propofol.pdf> (accessed 11.17.22).

Mizushima, M., Kawamura, T., Takahashi, K., Nitta, K.H., 2011. In situ near-infrared spectroscopic studies of the structural changes of polyethylene during melting. Polym. J. 2012 442 44, 162–166. doi: 10.1038/pj.2011.100.

Otto, F., Brezesinski, G., van Hoogevest, P., Neubert, R.H.H., 2018. Physicochemical characterization of natural phospholipid excipients with varying PC content. Colloids Surfaces A Physicochem. Eng. Asp. 558, 291–296. https://doi.org/10.1016/J.COLSURFA.2018.08.037.

Peeters, M., Lange, R., Aarts, L.P.H.J., Talsma, H., Knibbe, C., 2003. Stability of an intravenous fat emulsion containing 6% propofol and a low amount of emulsifier. Eur. J. Hosp. Pharm. 6, 1–8.

Placzek, M., Kosela, M., 2016. Microscopic methods in analysis of submicron phospholipid dispersions. Acta Pharm. 66, 1–22. https://doi.org/10.1515/ACPH-2016-0003.

Raman, M., Almutairdi, A., Mulesa, L., Alberda, C., Beattie, C., Gramlich, L., 2017. Parenteral nutrition and lipids. Nutrients 9. https://doi.org/10.3390/NU9040388.

Ratke, L., Thieringer, W.K., 1985. The influence of particle motion on Ostwald ripening in liquids. Acta Metall. 33, 1793–1802. https://doi.org/10.1016/0001-6160(85)90003-3.

Rotenberg, M., Rubin, M., Bor, A., Meyuhas, D., Talmon, Y., Lichtenberg, D., 1991. Physico-chemical characterization of Intralipid emulsions. Biochim. Biophys. Acta 1086, 265–272. https://doi.org/10.1016/0005-2760(91)90169-I.

Saad, M., Laghi, F.A., Brofman, J., Undevia, N.S., Shaikh, H., 2022. Long-term acute care hospital outcomes of mechanically ventilated patients with coronavirus disease 2019. Crit. Care Med. 50, 256–263. https://doi.org/10.1097/CCM.0000000000005193.

Schuurmans, C.L., Wijgergangs, J., Gerich, A., Besseling, R., 2022. Turbid Titanium Dioxide Nanosuspensions | Nanoflowsizer [WWW Document]. Available from: <https://www.azonano.com/article.aspx?ArticleID=5803&utm_source=researcher_app&utm_medium=referral&utm_campaign=RESR_MRKT_Researcher_inbound> (accessed 11.17.22).

Shang, Y., Pan, C., Yang, X., Zhong, M., Shang, X., Wu, Z., Yu, Z., Zhang, W., Zhong, Q., Zheng, X., Sang, L., Jiang, L., Zhang, J., Xiong, W., Liu, J., Chen, D., 2020. Management of critically ill patients with COVID-19 in ICU: statement from front-line intensive care experts in Wuhan, China. Ann. Intensive Care 101 (10) (2020) 1–24. doi: 10.1186/S13613-020-00689-1.

Tadros, T., 2013. Kelvin equation. Encycl. Colloid Interface Sci. 679–680. https://doi.org/10.1007/978-3-642-20665-8_112.

Thomas, J.C., 1987. The determination of log normal particle size distributions by dynamic light scattering. J. Colloid Interface Sci. 117, 187–192. https://doi.org/10.1016/0021-9797(87)90182-2.

Thompson, K.A., Goodale, D.B., 2000. The recent development of propofol (DIPRIVAN). Intensive Care Med. 26 (Suppl), 4. https://doi.org/10.1007/PL00003783.

United States Phamacopeial Convention, 2019. ⟨729⟩ Globule Size Distribution in Lipid Injectable Emulsions. In: United States Pharmacopeia. USP-NF, Rockville, MD. https://doi.org/10.31003/USPNF_M99505_02_01.

Wabel, C., 1998. Influence of Lecithin on Structure and Stability of Parenteral Fat Emulsions. Friedrich-Alexander-Universität Erlangen-Nürnberg, Erlangen-Nürnberg.

Walsh, C.T., 2018. Propofol: milk of amnesia. Cell 175, 10–13. https://doi.org/10.1016/J.CELL.2018.08.031.

Wang, D., Hu, B., Hu, C., Zhu, F., Liu, X., Zhang, J., Wang, B., Xiang, H., Cheng, Z., Xiong, Y., Zhao, Y., Li, Y., Wang, X., Peng, Z., 2020. Clinical characteristics of 138 hospitalized patients with 2019 novel coronavirus-infected pneumonia in Wuhan,. China. JAMA 323, 1061–1069. https://doi.org/10.1001/JAMA.2020.1585.

Wilson, R.H., Nadeau, K.P., Jaworski, F.B., Tromberg, B.J., Durkin, A.J., 2015. Review of short-wave infrared spectroscopy and imaging methods for biological tissue characterization. J. Biomed. Opt. 20, 030901 https://doi.org/10.1117/1.JBO.20.3.030901.

Wooster, T.J., Golding, M., Sanguansri, P., 2008. Impact of oil type on nanoemulsion formation and Ostwald ripening stability. Langmuir 24, 12758–12765. https://doi.org/10.1021/LA801685V.